

Regime shift increase in East Asia's summer extreme hot day frequency across the late 1990s

Yong-Han Lee¹ | Sang-Wook Yeh¹  | Jin-Sil Hong¹ | Jongsoo Shin² | Soon-Il An³ 

¹Department of Marine Science and Convergent Technology, Hanyang University, Ansan, South Korea

²Division of Environmental Science and Engineering, Pohang University of Science and Technology (POSTECH), Pohang, South Korea

³Department of Atmospheric Science, Yonsei University, Seoul, South Korea

Correspondence

Sang-Wook Yeh, Department of Marine Science and Convergent Technology, Hanyang University, Ansan 15588, South Korea.

Email: swyeh@hanyang.ac.kr

Funding information

National Research Foundation,
Grant/Award Numbers:
2021M316A1086803,
NRF2018R1A5A1024958

Abstract

Here we analysed the long-term change in extreme hot days (EHDs) in East Asia during boreal summer (June–July–August) since 1979, where EHDs was defined as days exceeding or equalling the 90th percentile threshold of the climatological (1991–2020) daily T_{\max} and T_{\min} . EHDs frequency occurrence in East Asia during summer showed not only an increasing trend but also a distinct regime shift increase since the late 1990s. Based on this regime shift, we divided these years into two periods, P1 (1979–1998) and P2 (1999–2021), and found that different physical processes operated for each period's EHDs variability. P2's EHDs was related to the stationary wave originating from both the North Atlantic Ocean and the Indo-Pacific warm pool, but these influences did not appear in P1. To investigate whether the observed regime shift increase was caused by natural variability or greenhouse gas concentration increases, we conducted a CO₂ quadrupling experiment as well as a present-day experiment with a fixed CO₂ concentration using the Community Earth System Model with 28 ensemble members. We demonstrated that the regime shift increase of East Asian EHDs occurrences was due to increasing greenhouse gas concentrations. We further discussed the influence of Arctic sea ice reduction due to global warming on EHDs occurrences in East Asia.

KEY WORDS

extreme hot days, increased CO₂, regime shift

1 | INTRODUCTION

In recent decades, the intensity, frequency, and duration of boreal summer (June–July–August, hereafter JJA) extreme high-temperature events such as heatwaves and tropical nights are gradually increasing. Previous literature suggested that these are mostly due to greenhouse gas concentration increases (Meehl and Tebaldi, 2004; Coumou and Rahmstorf, 2012; Perkins *et al.*, 2012; Yeh *et al.*, 2021). The areas where these extreme high-temperature events occur are not regionally limited; they

are widespread, encompassing most of the Northern Hemisphere including Europe, Russia, and East Asia (Kysely and Kim, 2009; Trenberth and Fasullo, 2012; Xia *et al.*, 2016; Yeh *et al.*, 2018; Xu *et al.*, 2020; Overland and Wang, 2021). Extreme high-temperature events can cause various diseases including convulsions, fainting, heat stroke, and even death. They can also have a large socio-economic impact (Luber and McGeehin, 2008).

East Asia includes China, Japan, and Korea and has a population of more than 1.6 billion (ESCAP, 2021). High-temperature events during JJA are responsible for

damage to this population (Min *et al.*, 2014; Zhou *et al.*, 2014; Ma *et al.*, 2017; Imada *et al.*, 2019). Hot days and warm nights have increased in most East Asian regions (Choi *et al.*, 2009; Hu and Huang, 2020; Yeh *et al.*, 2021). The high-temperature events, with characteristically high intensity and frequency, are largely influenced by atmospheric circulation changes and thermodynamic processes (Horton *et al.*, 2015; Vautard *et al.*, 2016; Ren *et al.*, 2020). Regional anticyclonic anomalies reduce cloud cover and increase downward short-wave radiation, leading to increased surface air temperature. This results in high-temperature events (Deng *et al.*, 2018; Hong *et al.*, 2018; Zhu and Li, 2018; Zhang *et al.*, 2020; Long *et al.*, 2022). Anticyclonic anomalies are caused from large-scale atmospheric circulation associating with an eastward-propagating wave train circum-global teleconnection and the Scandinavia teleconnection pattern. These teleconnections are associated with mid-latitude components that can affect the East Asian high-temperature events (Chen *et al.*, 2019; Kornhuber *et al.*, 2019; Choi *et al.*, 2020). Previous studies also suggest that large-scale circulation patterns such as the Pacific-Japan (PJ) pattern (Lee and Lee, 2016) originate from the western tropical Pacific and play a role in the high-temperature events. This means the high-temperature events are not only caused by thermodynamic processes but also by dynamic atmospheric circulation processes (Horton *et al.*, 2015; Vautard *et al.*, 2016; Zhu and Li, 2017; Yeo *et al.*, 2019; Ren *et al.*, 2020; Kim *et al.*, 2021).

East Asia's hot days and warm nights are caused by different physical mechanisms (Chen and Lu, 2014; Hong *et al.*, 2018). While hot days are attributed to short-wave radiation, warm nights are caused by warm humid air, cloud cover, and long-wave radiation (Chen and Lu, 2014; Hong *et al.*, 2018). Few studies, however, have investigated the physical processes associated with compounding both hot days and warm nights. In this study, we analyse the characteristics of East Asia's JJA extreme hot days (EHDs), when both hot days and warm nights occur simultaneously. Some studies argue that East Asia's hot days are closely related to the circum-global teleconnection before the mid-1990s, while the Scandinavia teleconnection pattern explains the more recent occurrences (Choi *et al.*, 2020). This implies significant atmospheric circulation changes, and there are different atmospheric circulation patterns associated with East Asian heatwave occurrences before and after 1999. Further analysis is still necessary, however, to understand the physical processes leading to these compounding events. Unless stated otherwise in the text, the results are for the summer (JJA) season only.

In this paper, section 2 describes our data and methodology. Section 3 explains the EHDs frequency during East Asian summers and compares each period's characteristics. Section 4 discusses and summarizes the study.

2 | DATA AND METHODOLOGY

2.1 | Observational and reanalysis datasets

Daily temperature and outgoing long-wave radiation (OLR) records are from the Climate Prediction Center dataset from 1979 to 2021. This dataset was developed by the American National Oceanic and Atmospheric Administration (NOAA). The dataset's maximum temperature (T_{\max}) and minimum temperature (T_{\min}) have a horizontal resolution of $0.5^\circ \times 0.5^\circ$ and for the average temperature, the average of the T_{\max} and T_{\min} was calculated and used. We interpolated the monthly OLR gridded data to $2.5^\circ \times 2.5^\circ$. The monthly sea surface temperature (SST) and sea ice concentration (SIC) dataset from the Hadley Center Sea Ice and SST (HadISST) have a horizontal resolution of $1.0^\circ \times 1.0^\circ$ (Rayner *et al.*, 2003). To increase the reliability and certainty of results derived from the CPC datasets, we also analysed T_{\max} and T_{\min} records from the Gridded Berkeley Earth Surface Temperature (Muller *et al.*, 2013). The other atmospheric variables are obtained from the version 5 of the European Centre for Medium-Range Weather Forecasts Reanalysis (ERA5) with a horizontal resolution of a $2.5^\circ \times 2.5^\circ$ and 17 pressure levels which is available by the European Center for Medium-Range Weather Forecasts (ECMWF) (Hersbach *et al.*, 2020). The datasets' time period covers the same range as the observational data.

2.2 | Definition of extreme hot days

There are several ways to define extreme hot days (EHDs) according to previous literature. It can be used as either an absolute reference value or a relative value (Park *et al.*, 2008; Perkins and Alexander, 2013). We defined EHDs by obtaining the 90th percentile of the local temperature. Thresholds were calculated based on the 90th percentile of climatological (1991–2020) daily T_{\max} and T_{\min} at each grid point. EHDs were defined as the days when both T_{\max} and T_{\min} were equal to or exceeded the threshold (Table 1). In a previous study, days when T_{\max} and T_{\min} were equal to or exceeded the threshold were defined as Hot Day and

TABLE 1 Extreme hot days (EHDs) definition

EHDs	
Definition	$T_{\max} \geq 90$ th percentile threshold of climatological T_{\max}
	$T_{\min} \geq 90$ th percentile threshold of climatological T_{\min}

Warm Night, respectively (Yeh *et al.*, 2021). We would like to define the days when these two occur simultaneously as EHDs. We calculated the EHDs frequency mean for each grid from 1979 to 2021 during JJA. We averaged the EHDs frequency for East Asia (20° – 50° N, 100° – 145° E) according to the IPCC report (Iturbide *et al.*, 2020).

2.3 | Regime shift analysis

For regime shift analysis, we used a method developed by Rodionov (Rodionov, 2004). Regime shift detection details are available at the webpage (<https://sites.google.com/view/regime-shift-test/home>). Rodionov (2004) used a sequential data processing technique in which the number of observations is not fixed to solve a common problem in which statistics tends to deteriorate the end of the time series in previous regime shift methods (Easterling and Peterson, 1995; Lanzante, 1996). We applied this method to the EHDs frequency time series. The significance level was calculated using a 2-tailed *t* test and adjusted for serial correlation using the equivalent sample size technique (von Storch, 1999; Rodionov, 2006). If there were less than 15 years left before and after a regime shift year, we omitted the case. This is because a regime shift requires an abrupt transition from one quasi-steady climate state (15–20 years) to another and a transition period should be much shorter than the length of the individual epochs (Hong and Wu, 2018). We used the 99% confidence level as the significant difference between the mean values of neighbouring regimes.

2.4 | Wave activity flux analysis

The wave activity flux (WAF) (Takaya and Nakamura, 1997, 2001) was used to examine the distribution of stationary Rossby wave train propagation. The methodology is available at https://github.com/laishenggx/T-N_Wave-Activity-Flux. The horizontal WAF is defined as follows:

$$W = \frac{p \cos \phi}{2|U|} \left[\begin{array}{l} \frac{U}{a^2 \cos^2 \phi} \left\{ \left(\frac{\partial \psi'}{\partial \lambda} \right)^2 - \psi' \frac{\partial^2 \psi'}{\partial \lambda^2} \right\} \\ + \frac{V}{a^2 \cos \phi} \left\{ \frac{\partial \psi'}{\partial \lambda} \frac{\partial \psi'}{\partial \phi} - \psi' \frac{\partial^2 \psi'}{\partial \lambda \partial \phi} \right\} \\ \frac{U}{a^2 \cos \phi} \left\{ \frac{\partial \psi'}{\partial \lambda} \frac{\partial \psi'}{\partial \phi} - \psi' \frac{\partial^2 \psi'}{\partial \lambda \partial \phi} \right\} \\ + \frac{V}{a^2} \left\{ \left(\frac{\partial \psi'}{\partial \lambda} \right)^2 - \psi' \frac{\partial^2 \psi'}{\partial \phi^2} \right\} \end{array} \right]. \quad (1)$$

The variables $a (= 6.37 \times 10^6 \text{ m})$, ϕ , and λ denote the Earth's radius, latitude, and longitude, respectively. The variables p , U , and V represent the climatology of geopotential, zonal wind, and meridional wind at the 200 hPa level, respectively. The geostrophic stream function perturbation is defined as

$$\psi' = \frac{g}{f} \phi', \quad (2)$$

where ϕ' is geopotential regressed on EHDs frequency for 1979–2021, $g (= 9.81 \text{ m}^2 \cdot \text{s}^{-2})$ is the gravitational acceleration, and $f (= 2\Omega \sin \phi)$ is the Coriolis parameter with the Earth's rotation rate $\Omega (= 7.29 \times 10^{-5} \text{ rads}^{-1})$. We first calculated the regressed anomaly of every field in Equation (1) and then calculated WAF using Equation (1).

2.5 | Community Earth System Model (CESM1.2.2) experiment

To determine whether the EHDs regime shift is induced by greenhouse gas concentration increases, we used the Community Earth System Model version 1.2.2 (CESM1.2.2) (Hurrell *et al.*, 2013). CESM1.2.2 consists of the atmosphere (The Community Atmospheric Model version 5, CAM5), ocean (The Parallel Ocean Program version 2, POP2), sea ice (The Community Ice Code version 4, CICE4), and land models (Community Land Model version 4, CLM4). CAM5 has a horizontal resolution of 0.9° latitude by 1.25° longitude and 30 vertical levels (Neale *et al.*, 2012). POP2 has 60 vertical levels with longitudinal 1° and latitudinal 0.3° resolutions that gradually increase to 0.5° from the equator to the poles (Smith *et al.*, 2010). CLM4 includes the carbon–nitrogen cycle (Lawrence *et al.*, 2011). CESM1.2.2 has been used to assess the trends of mean and extreme temperature and precipitation over East Asia. Li *et al.* (2017) showed that CESM large ensemble models can

capture the trends of observed annual mean temperature and extremely low-temperature days of China. In addition, Dong *et al.* (2021) investigated three characteristics of heatwaves including frequency, duration and amplitude in Southeast Asia in both the observations and CESM and showed that some characteristics of heatwaves over Southeast Asia are reproduced well in CESM along with the increased global mean surface temperature in the past decades and in a warmer world.

We conducted two simulations: one where the atmospheric CO₂ concentration is fixed at present-day 367 ppm for the 899-year simulation period (referred to as the present-day [PD] experiment), and the other where the atmospheric CO₂ content increased by 1% per year for 140 years until it quadrupled to 1,468 ppm. This simulation is referred to as the 4 × CO₂ experiment with 28 ensemble members.

3 | RESULTS

3.1 | EHDs frequency in East Asia from 1979 to 2021

Figure 1a displays EHDs frequency in East Asia from 1979 to 2021. The most striking feature is that EHDs frequency has a significant upward trend of 0.23 days·month⁻¹·decade⁻¹ for the entire period with statistical significance at the 99% confidence level. Furthermore, EHDs occurrences increase suddenly after the late 1990s based on a regime shift analysis (Figure 1b). This implies the EHDs frequency experienced a regime-shift after 1999. Based on this information, we divided our experiments into two time periods: 1979–1998 (P1 period) and 1999–2021 (P2 period).

The averaged EHDs frequencies for P1 and P2 are 0.6 and 1.3 days·month⁻¹, respectively. There is no significant upward or downward trend in EHDs occurrences within P1 and P2, respectively. In addition, EHDs occurrence variability during P2 is much greater than during P1 (Table 2), implying that both EHDs occurrence mean, and variance has changed significantly from P1 to P2. To confirm this, we also calculated EHDs frequency using the Berkeley Earth Surface Temperature datasets (Muller *et al.*, 2013) to compare with the CPC datasets. Despite some discrepancies between the two datasets, the two time series are highly correlated with a statistically significant correlation of 0.7 at the 99% confidence level along with a regime-shift increase after the late 1990s (Figure 1c).

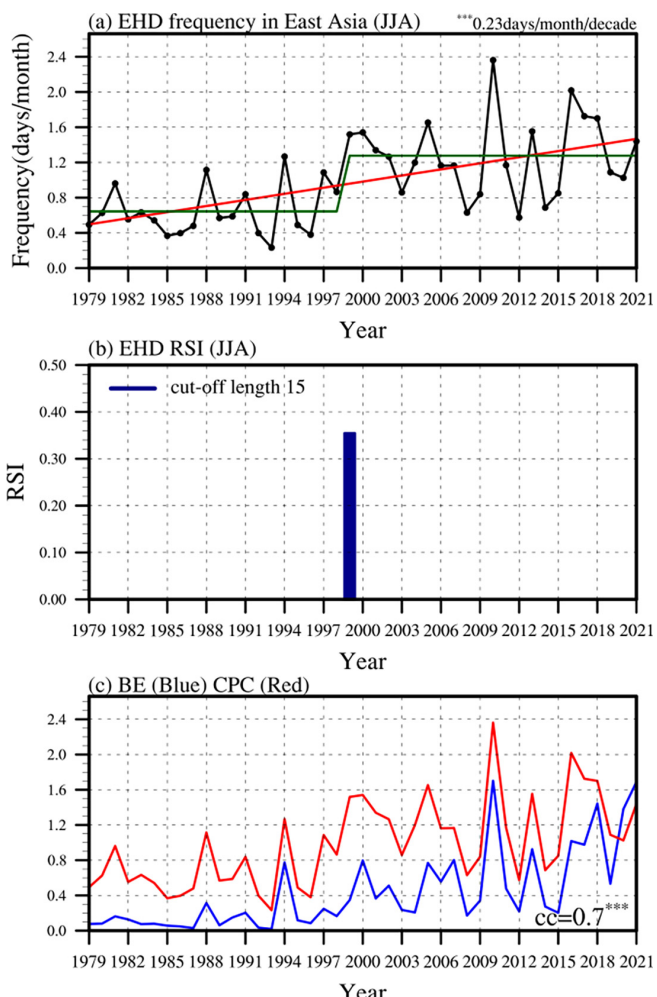
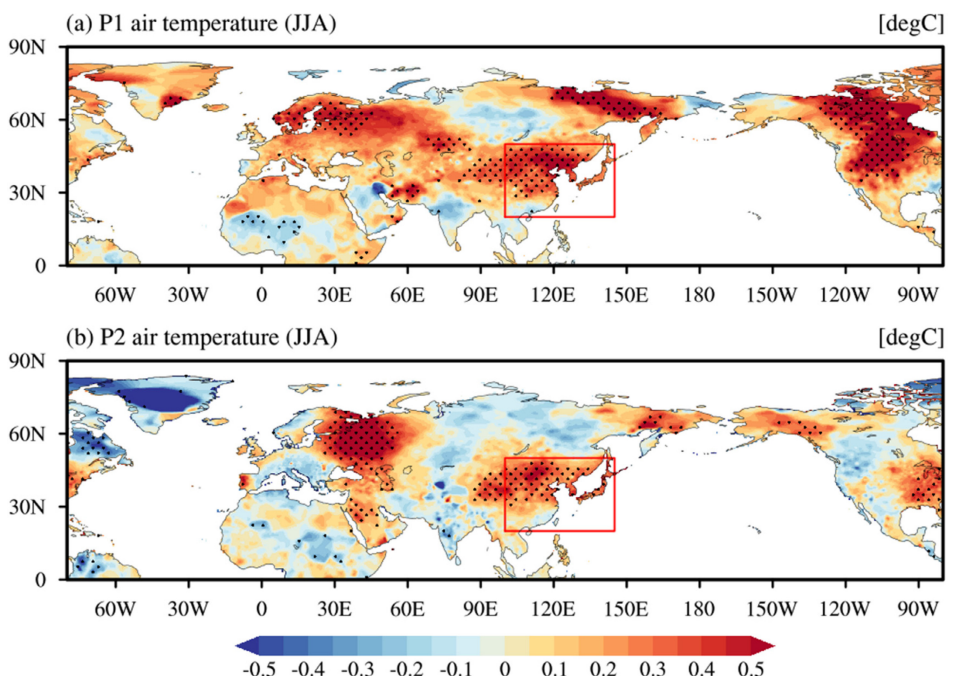


FIGURE 1 (a) Monthly mean EHDs frequency for JJA, 1979–2021. The red line indicates a linear trend and the green line denotes each regime's mean value. The value in the upper right corner is the linear trend's regression coefficient. The 99% statistical significance level is marked by ***. (b) EHDs frequency regime shift index for JJA, 1979–2021. The following parameters were used to determine the regime shift: probability level 0.01, cut-off length 15, and Huber's weight parameter 1.0. (c) EHDs occurrences calculated for 1979–2021 using CPC datasets (red dashed line, right y-axis) and Berkeley Earth datasets (BE) (blue line, left y-axis). “cc” is the two indices' correlation coefficient. The 99% statistical significance level is marked by *** [Colour figure can be viewed at wileyonlinelibrary.com]

TABLE 2 EHDs linear trend and standard deviation frequency for P1 (1979–1998) and P2 (1999–2021)

	P1 (1979–1998)	P2 (1999–2021)
Trend in EHDs frequency (days·month ⁻¹ ·decade ⁻¹)	0.09	0.02
Standard deviation	0.28	0.45

FIGURE 2 Regressed surface air temperature anomaly against with the EHDs variability for period P1 (a) and P2 (b). The black dots indicate 95% confidence level areas. The anomalies were calculated by subtracting P1 (a) and P2 (b) climatology. Red box in -denotes East Asia region (20° – 50° N, 100° – 145° E) [Colour figure can be viewed at wileyonlinelibrary.com]



3.2 | Changes in the physical factors leading to EHDs occurrences in the late 1990s

In this subsection, we examined atmosphere and ocean variables associated with EHDs variability using the regressed analysis. We removed the EHDs frequency's linear trend and standardized to obtain the regressed variables. The regressed results indicate how atmosphere and ocean are associated with EHDs variability during P1 and P2.

Figure 2a,b displays the regressed surface air temperature against with the EHDs variability for P1 and P2, respectively. Surface warming is evident in East Asia during both periods, implying as suggested in previous studies, that the increase in land surface temperature is closely linked to EHDs occurrences (Collins *et al.*, 2000; Peterson *et al.*, 2008; Perkins *et al.*, 2012; Wang *et al.*, 2020). Frequent EHDs occurrences during P1 are linked with the land surface warming in central and East Asia along with North America (Figure 2a). During P2, however, it is connected to Eastern Europe (Figure 2b), where the land surface warming structure is characterized by a wave-like pattern from Europe to East Asia. Frequent EHDs occurrences during P1 are concurrent with North American warming; this is not seen during P2. This result implies there may be mechanism differences contributing to EHDs occurrences during the two periods.

To examine this, we plotted the regressed SST anomalies against EHDs frequency for P1 and P2 (Figure 3). Results show large SST condition discrepancies

associated with EHDs occurrences between the two periods. While the frequent EHDs occurrences during P1 are closely associated with SST warming extending from the western to central North Pacific (Figure 3a), a La Niña-like structure is dominant during P2 (Figure 3b). This is in contrast with the Indian Ocean's SST warming structure, which has only a limited statistical significance during P1 (Figure 3a). EHDs variability during P1 has no significant relationship with tropical SSTs except in very limited regions (Figure 3a). The correlation between the western North Atlantic Ocean and EHDs variability is statistically significant during P1 while during P2, it is eastern North Atlantic Ocean's dipole-like anomalous SST structure that significantly relates to EHDs variability (Figure 3a,b). While our regression analysis does not imply the causality, we inferred that SST forcing, which is conducive to the frequent EHDs occurrences in East Asia, is not the same during P1 and P2.

To further investigate the contrasting processes associated with EHDs variability between P1 and P2, we examined the regressed geopotential height and horizontal wave activity flux in the upper atmosphere (200 hPa) (Figure 4). During both P1 and P2, EHDs occurrences are closely related to anomalous upper atmosphere anticyclonic circulation over East Asia (Figure 4a,b). This is consistent with previous studies (Hong *et al.*, 2018; Hu and Huang, 2020; Ren *et al.*, 2020). The most striking difference between the two periods is that the horizontal stationary wave train from the North Atlantic to East Asia is much more prominent in the upper atmosphere during P2 (Figure 4b) than during P1 (Figure 4a). This implies that SST forcing in the eastern North Atlantic

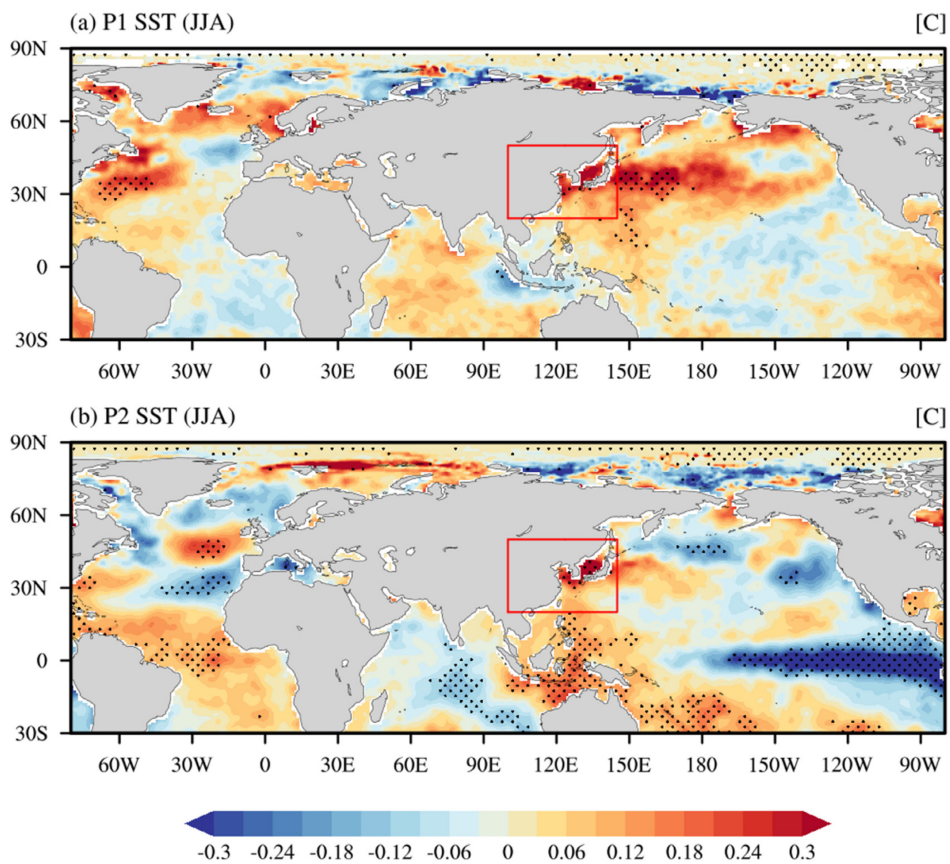


FIGURE 3 Same as Figure 2, except for SST [Colour figure can be viewed at wileyonlinelibrary.com]

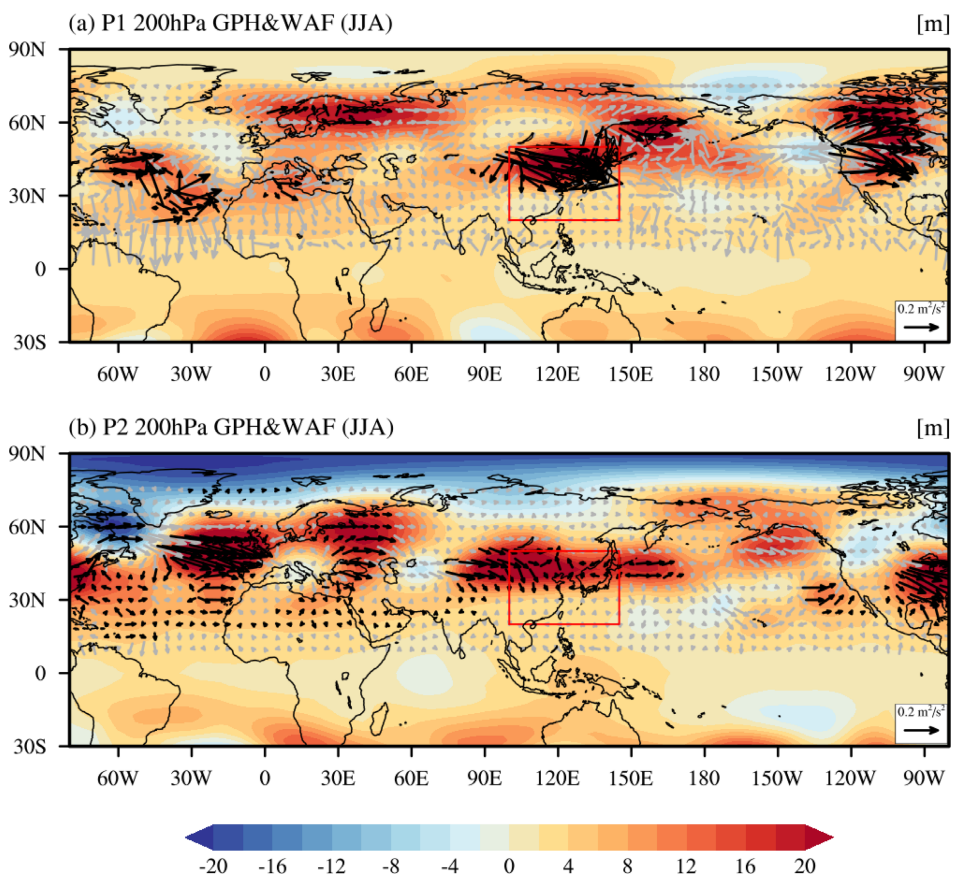


FIGURE 4 Same as Figure 2, except for geopotential height (contour, meter) and wave activity flux (vector, $\text{m}^2 \cdot \text{s}^{-2}$) at 200 hPa. The black vectors denote 95% confidence level areas [Colour figure can be viewed at wileyonlinelibrary.com]

FIGURE 5 (a) Regressed geopotential height (shading) and wave activity flux (arrow) against with the SST anomalies averaged in the western North Atlantic Ocean (45° – 75° W, 25° – 40° N) (blue box) during P1 (1979–1998). The black colour in vectors denotes the 95% confidence level. The anomalies were calculated by subtracting P1 climatology. Blue and red box denotes the western North Atlantic and the East Asian region, respectively. Units in geopotential height and wave activity flux are meter and $\text{m}^2 \cdot \text{s}^{-2}$, respectively. (b) The blue bars show a 21-year moving correlation of SST anomalies in the western North Pacific and East Asian EHDs variability for 1979–2021. Straight solid line denotes the statistical significance at the 95% confidence level [Colour figure can be viewed at wileyonlinelibrary.com]

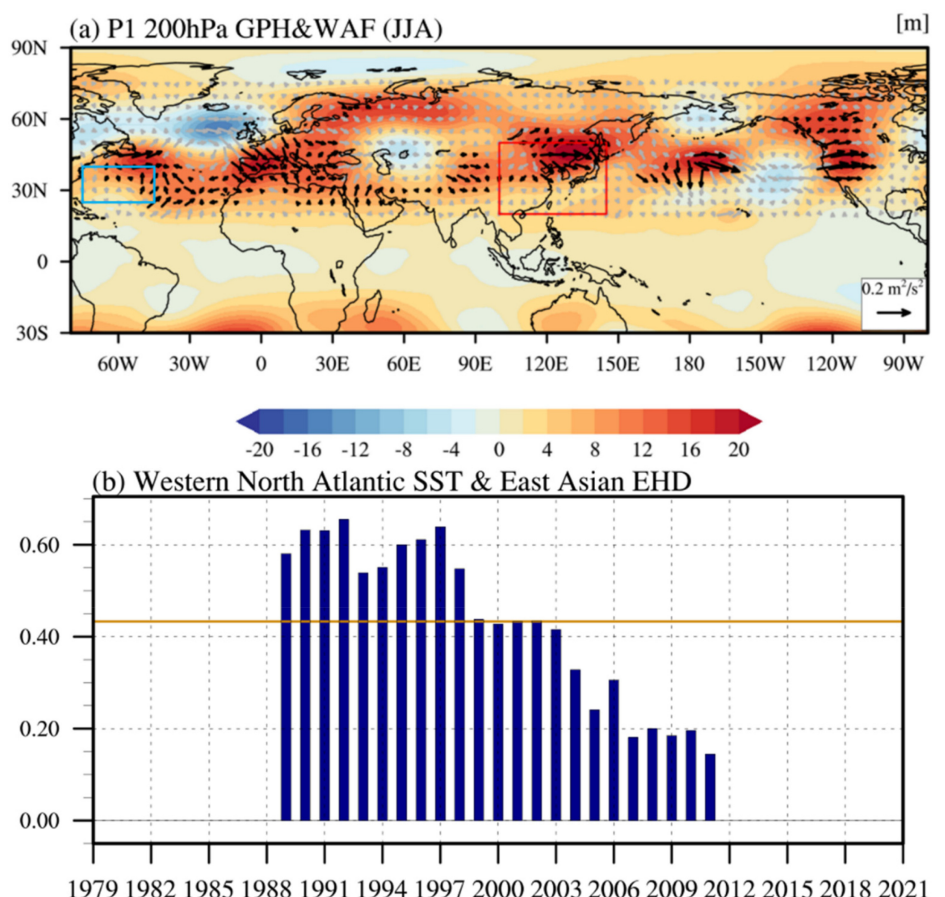
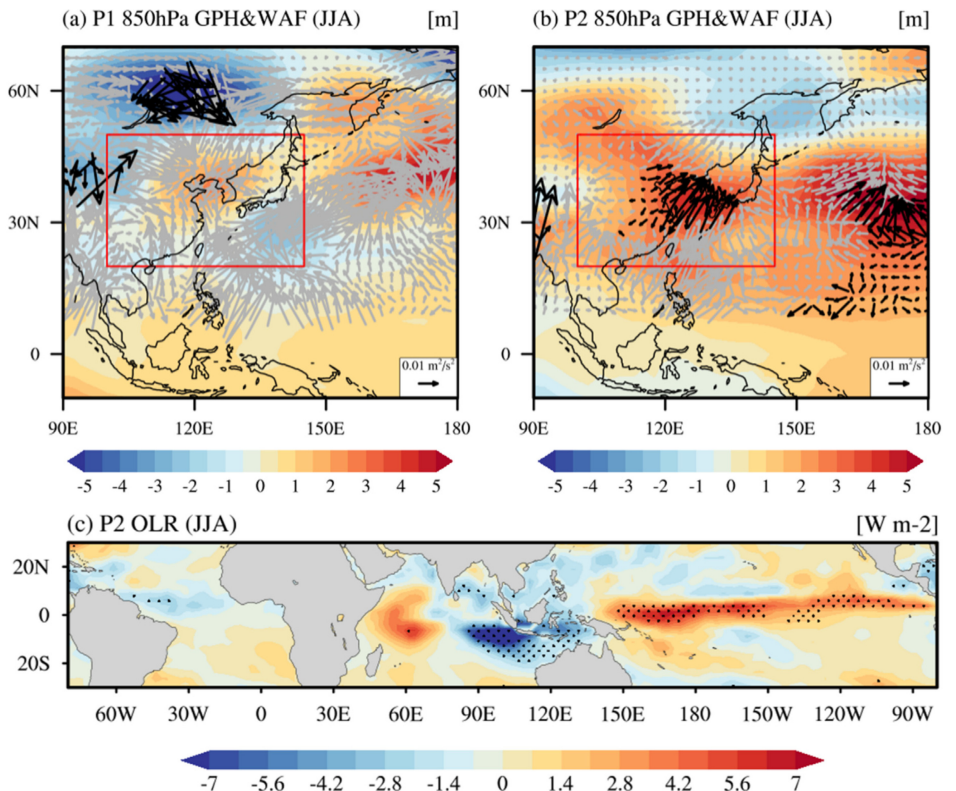


FIGURE 6 (a, b) Same as Figure 4a,b except at 850 hPa. (c) Indicates the regressed outgoing long-wave radiation (OLR) anomalies against with the EHDs variability during P2. The black dots indicate the statistical significant region at the 95% confidence level. The OLR anomalies were calculated by subtracting the climatology during P2 [Colour figure can be viewed at wileyonlinelibrary.com]



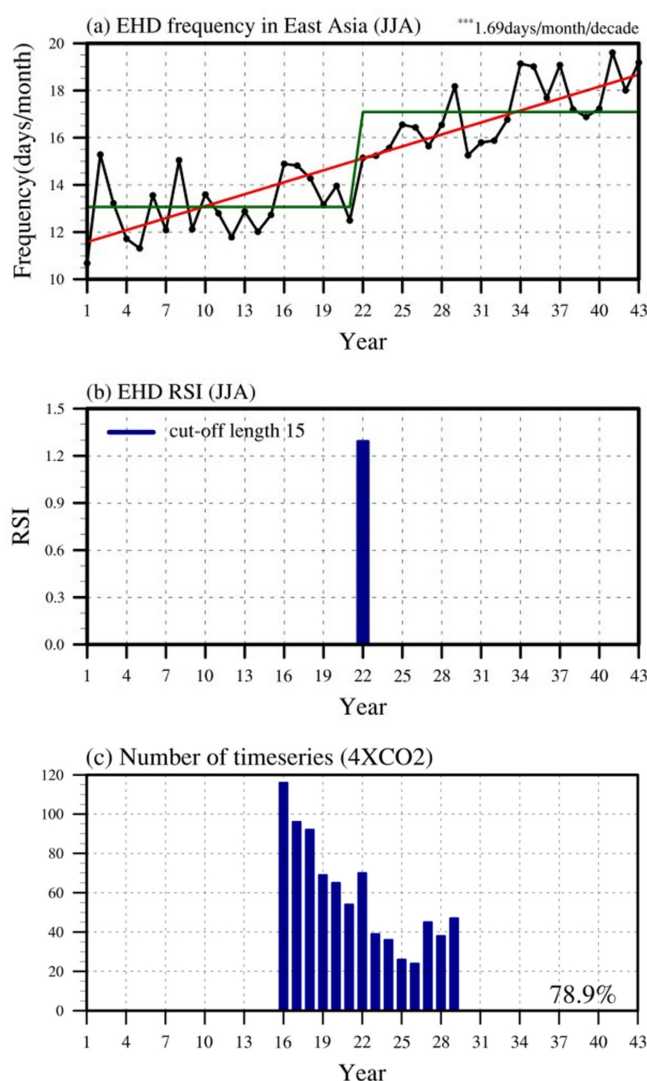


FIGURE 7 (a, b) Same as Figure 1a,b, but for a single time series in the randomly chosen 43-year period in the $4 \times CO_2$ experiment. (c) The number of regime shift occurrences (y-axis) based on the year (x-axis) in the $4 \times CO_2$ experiment [Colour figure can be viewed at wileyonlinelibrary.com]

Ocean (Figure 3b), which induces the zonally oriented horizontal stationary wave train, plays a role in EHDs occurrences during P2. This is not seen during P1. In spite of this, however, we argue that the anticyclone anomaly in East Asia during P1 (Figure 4a) could be caused by the zonal wave train forced by the positive SST anomalies in the western North Atlantic (Figure 5a). There is a wave train originated from the western North Atlantic Ocean into East Asia along with the anticyclonic circulation over East Asia, implying that the western North Atlantic SST plays a role to induce the atmospheric teleconnections into East Asia during P1. Our further analysis indicates that the western North Atlantic SST variability had significantly correlated with East Asian

EHD variability in the past, that is, during P1, but has weakened in recent decades (Figure 5b). This implies that there was a distinctly different relationship between the western North Atlantic SST and East Asian EHD frequencies during the periods of P1 and P2, respectively.

We also analysed atmospheric circulation and horizontal wave flux at a lower atmospheric level (850 hPa) to examine the role of tropical forcing on EHDs variability (Figure 6a,b). We found that the meridional stationary wave train, originating from the Indo-Pacific warm pool, is dominant during P2 (Figure 6b). This contrasts with that during P1 (Figure 6a). Note that the reason of why there is no significant wave activity flux originating from the eastern Indian Ocean and the Maritime Continent during P1 and P2 is because the WAF is very weak at low latitudes where the Coriolis force is very small. Figure 6c shows the regressed OLR anomalies against EHDs variability. Negative regressed OLR anomalies in the Indian Ocean represent the increased convection there. An increased convective forcing acts to induce the meridional atmospheric teleconnections from Indian Ocean to East Asia, which contributes to the occurrence of EHDs in conjunction with anomalous anticyclonic circulation during P2. Therefore, we infer that tropical SST forcing including the Indian Ocean, which induces the meridional atmospheric teleconnections into East Asia, significantly contributes to East Asian EHDs occurrences with its increased variability during P2.

3.3 | Climate model experiments using CESM1.2.2

The regime shift increase in East Asian EHDs occurrences could be due to natural variability, anthropogenic forcing, or some combination of the two. In order to examine this, we analysed daily T_{\max} and T_{\min} datasets simulated in the PD experiment over an 899-year period and the $4 \times CO_2$ experiment with 28 ensembles over a 140-year period. We chose a 43-year period, which is the same period as the observations (1979–2021), for both the PD and $4 \times CO_2$ experiments. We then calculated EHDs occurrences with a regime shift analysis for each 43-year chunk in the two experiments. We conducted the same analysis 1,000 times.

Figure 7a displays a randomly chosen single set of the EHDs occurrence time series obtained from the $4 \times CO_2$ experiment. Similar to the observational data (Figure 1a), EHDs frequency simulated in the $4 \times CO_2$ experiment has a significant upward trend of $0.17 \text{ days} \cdot \text{month}^{-1} \cdot \text{year}^{-1}$ during the 43-year randomly chunk with a statistical significance at the 99% confidence level. The simulated EHDs occurrences

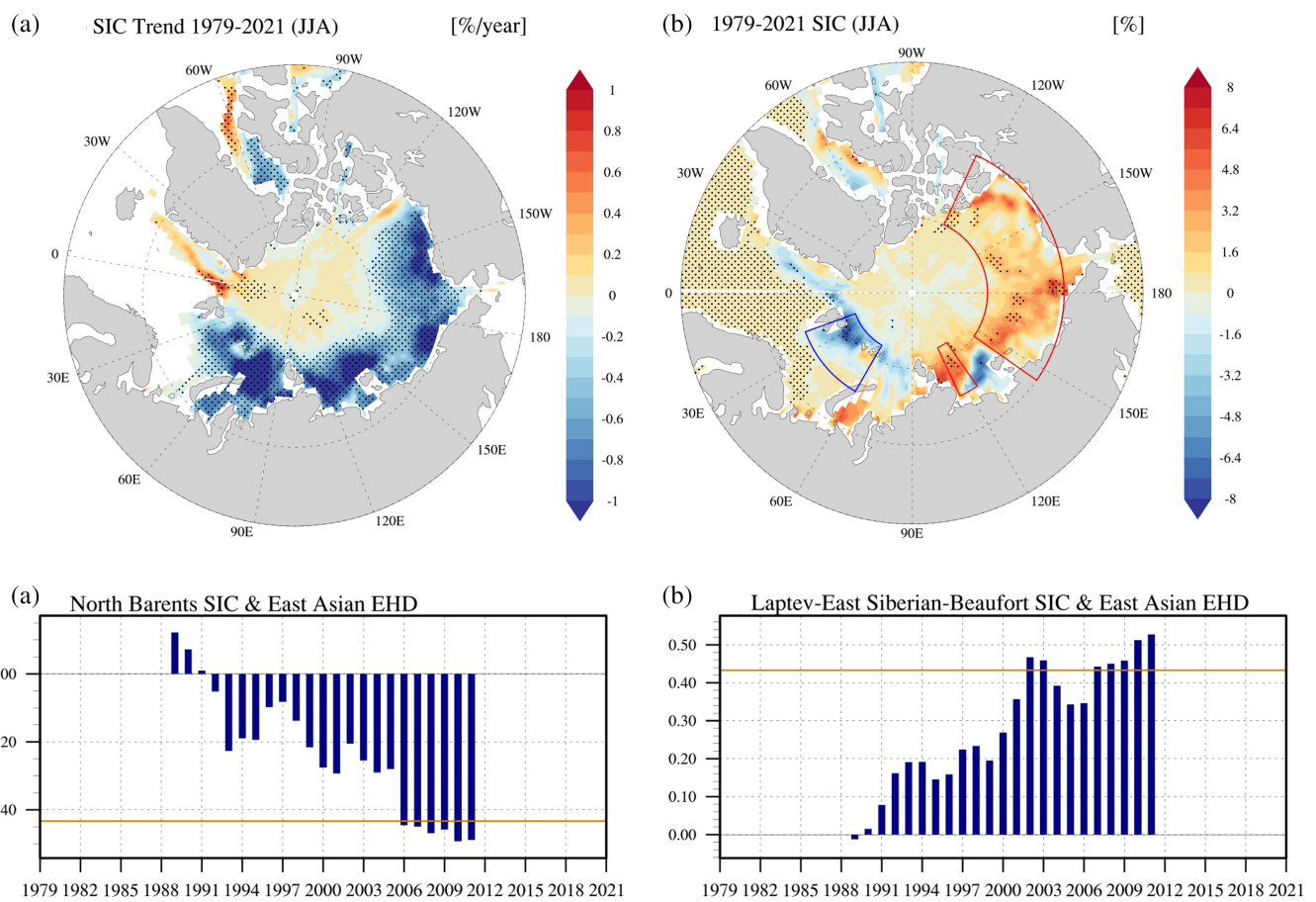


FIGURE 8 (a) Arctic SIC trends for 1979–2021. The dotted region denotes the area where the statistical significance is above the 95% confidence level. (b) Regressed SIC anomalies against with the EHDs occurrences for 1979–2021. The dotted region denotes the area where the statistical significance is above the 95% confidence level. (c) The blue bars show a 21-year moving correlation of SIC anomalies averaged in Barents Sea (75° – 82° N, 20° – 60° E) and EHDs variability. (d) Same as in (c) except for the SIC anomalies averaged in the Laptev Sea (75° – 82° N, 115° – 125° E), East Siberian Sea and Beaufort Sea (70° – 80° N, 145° – 245° E). The yellow line denotes the statistical significance at the 95% level [Colour figure can be viewed at wileyonlinelibrary.com]

suddenly increase in the middle period based on regime shift analysis (Figure 7b).

We conducted the regime shift analysis on two 1,000 sets for a randomly chosen 43-year period in the PD and $4 \times \text{CO}_2$ experiment, respectively. Results showed no regime shift increase in the PD experiment (figure not shown). In contrast, a regime shift-like increase in EHDs frequency occurs in 789 (78.9%) out of 1,000 sets in the $4 \times \text{CO}_2$ experiment (Figure 7c). Figure 7c shows the number of regime shift occurrences based on the year. While there is a diversity of years when the regime shift occurs, regime shift occurrence is detected from the early to late period of the 43-year chunk in the $4 \times \text{CO}_2$ experiment. This result shows that the observational regime shift-like increase of EHDs occurrences in East Asia is likely due to greenhouse gas concentration increases.

4 | DISCUSSION AND SUMMARY

The frequency of boreal summer extreme high temperatures, such as heatwaves and tropical nights, is rapidly increasing and has a significant impact on human activity and socioeconomic conditions. In this study, we analysed the physical processes leading to both hot days and warm nights in East Asia during JJA. We found that East Asian EHDs occurrences experienced a regime-shift-like increase after 1999 with different controlling factors on its variability than earlier time periods. P1 EHDs variability has no significant relationship with tropical SST except in very limited regions while a La Niña-like structure is dominant during P2. In addition, the horizontal stationary wave train from the North Atlantic to East Asia and from the Indo-Pacific warm pool to East Asia are much more prominent at upper atmospheric levels

during P2 than during P1. This indicates that SST forcing in both the eastern North Atlantic Ocean and the Indo-Pacific warm pool plays a role in EHDs occurrences in East Asia during P2. Therefore, we argue that the controlling factors leading to EHDs occurrences in East Asia have changed since the late 1990s.

According to previous studies (Luo and Lau, 2019; 2020; Lee *et al.*, 2021), on the other hand, the occurrence of extreme high-temperature events such as EHD in East Asia is closely related to El Niño and Southern Oscillation (ENSO) with modulating circumglobal teleconnection and the strength of western North Pacific subtropical high. Indeed, there is a clear difference not only in the Atlantic oceans but also in ENSO monitoring regions, which is associated with the EHD occurrence between the two periods (see Figure 3). Therefore, we speculate that the role of SST forcing in the eastern tropical Pacific on the EHDs occurrence in East Asia has been changes from P1 to P2.

In addition, our two experiments using the CESM1.2.2 indicate that a regime shift-like increase in EHDs occurrences is likely due to increased CO₂ concentrations. We did not examine the details of how increased CO₂ concentrations cause this regime shift-like increase of EHDs occurrences. We inferred that Arctic sea ice reduction, which could be due to either global warming due to the increase of CO₂ concentrations (Vinnikov *et al.*, 1999) or internal variability (England *et al.*, 2019), or their combined influences, may affect EHDs frequency and may contribute to the regime shift-like increase.

Figure 8a,b compared the linear trend of SIC in the Arctic and regressed SIC anomalies with EHDs occurrences between 1979 and 2021 (Figure 8a,b). There are regions where the SIC is significantly reduced as time progresses and the SIC variability is significantly correlated with the EHDs variability in the Arctic. We selected two regions, one is Barents Sea (75°–82°N, 20°–60°E) where the SIC is significantly reduced (Figure 8a) and the SIC variability is negatively correlated with the EHDs variability (Figure 8b). The other is the Laptev Sea (75°–82°N, 115°–125°E), East Siberian Sea and Beaufort Sea (70°–80°N, 145°–245°E) where the SIC is significantly reduced (Figure 8a) and the SIC variability is positively correlated with the EHDs variability (Figure 8b). A 21-year moving correlation between East Asian EHDs occurrences and SIC in the Barents Sea clearly shows that their relationship significantly increases during P2 (Figure 8c). A similar phenomenon is observed in a 21-year moving correlation between East Asian EHDs occurrences and SIC in the Laptev Sea, East Siberian Sea, and Beaufort Sea (Figure 8d). Therefore, we speculated that SIC reduction in the Arctic may contribute to the variability of East Asian EHDs during P2 and to P2's

regime shift increase in EHDs occurrences. However, it is necessary to carefully examine how either global warming and its associated Arctic sea ice reduction or change in atmospheric circulation relatively contributes to the regime shift increase of EHD occurrence in East Asia.

AUTHOR CONTRIBUTIONS

Yong-Han Lee: Conceptualization; formal analysis; investigation; writing – original draft. **Jin-Sil Hong:** Investigation. **Jongsoo Shin:** Methodology. **Soon-Il An:** Writing – review and editing.

ACKNOWLEDGEMENTS

The CESM simulation was carried out on the supercomputer supported by the National Center for Meteorological Supercomputer of Korea Meteorological Administration (KMA), the National Supercomputing Center with supercomputing resources, associated technical support (KSC-2019-CHA-0005), and the Korea Research Environment Open NETwork (KREONET). This work was supported by National Research Foundation (Grant NRF2018R1A5A1024958). Sang-Wook Yeh is also supported by the research program for the carbon cycle between ocean, land and atmosphere of the National Research Foundation (NRF) funded by the Ministry of Science and Information and Communication Technologies (2021M316A1086803).

ORCID

Sang-Wook Yeh  <https://orcid.org/0000-0003-4549-1686>
Soon-Il An  <https://orcid.org/0000-0002-0003-429X>

REFERENCES

- Chen, H., He, D. and Zhu, Z. (2019) The internal multidecadal variability of SST in the Pacific and its impact on air temperature and rainfall over land in the Northern Hemisphere. *Atmosphere*, 10(3), 153. <https://doi.org/10.3390/atmos10030153>.
- Chen, R. and Lu, R. (2014) Dry tropical nights and wet extreme heat in Beijing: atypical configurations between high temperature and humidity. *Monthly Weather Review*, 142(5), 1792–1802. <https://doi.org/10.1175/MWR-D-13-00289.1>.
- Choi, G., Collins, D., Ren, G., Trewin, B., Baldi, M., Fukuda, Y., Afzaal, M., Pianmana, T., Gomboluudev, P., Huong, P.T.T., Lias, N., Kwon, W.-T., Boo, K.-O., Cha, Y.-M. and Zhou, Y. (2009) Changes in means and extreme events of temperature and precipitation in the Asia-Pacific Network region, 1955–2007. *International Journal of Climatology*, 29(13), 1906–1925. <https://doi.org/10.1002/joc.1979>.
- Choi, N., Lee, M.-I., Cha, D.-H., Lim, Y.-K. and Kim, K.-M. (2020) Decadal changes in the interannual variability of heat waves in East Asia caused by atmospheric teleconnection changes. *Journal of Climate*, 33(4), 1505–1522. <https://doi.org/10.1175/JCLI-D-19-0222.1>.
- Collins, D.A., Della-Marta, P.M., Plummer, N. and Trewin, B.C. (2000) Trends in annual frequencies of extreme temperature

- events in Australia. *Australian Meteorological Magazine*, 49(4), 277–292.
- Coumou, D. and Rahmstorf, S. (2012) A decade of weather extremes. *Nature Climate Change*, 2(7), 491–496. <https://doi.org/10.1038/nclimate1452>.
- Deng, K., Yang, S., Ting, M., Lin, A. and Wang, Z. (2018) An intensified mode of variability modulating the summer heat waves in eastern Europe and northern China. *Geophysical Research Letters*, 45(20), 11361–11369. <https://doi.org/10.1029/2018GL079836>.
- Dong, Z., Wang, L., Sun, Y., Hu, T., Limsakul, A., Singhru, P. and Pimonsree, S. (2021) Heatwaves in Southeast Asia and their changes in a warmer world. *Earth's Future*, 9(7), e2021EF001992. <https://doi.org/10.1029/2021EF001992>.
- Easterling, D.R. and Peterson, T.C. (1995) A new method for detecting undocumented discontinuities in climatological time series. *International Journal of Climatology*, 15(4), 369–377. <https://doi.org/10.1002/joc.3370150403>.
- England, M., Jahn, A. and Polvani, L. (2019) Nonuniform contribution of internal variability to recent Arctic Sea ice loss. *Journal of Climate*, 32(13), 4039–4053. <https://doi.org/10.1175/JCLI-D-18-0864.1>.
- ESCAP. (2021) *ESCAP population data sheet 2021: population and development indicators for asia and the Pacific*. Bangkok: UNESCAP.
- Hersbach, H., Bell, B., Berrisford, P., Hirahara, S., Horányi, A., Muñoz-Sabater, J., Nicolas, J., Peubey, C., Radu, R., Schepers, D., Simmons, A., Soci, C., Abdalla, S., Abellán, X., Balsamo, G., Bechtold, P., Biavati, G., Bidlot, J., Bonavita, M., de Chiara, G., Dahlgren, P., Dee, D., Diamantakis, M., Dragani, R., Flemming, J., Forbes, R., Fuentes, M., Geer, A., Haimberger, L., Healy, S., Hogan, R.J., Hólm, E., Janisková, M., Keeley, S., Laloyaux, P., Lopez, P., Lupu, C., Radnoti, G., de Rosnay, P., Rozum, I., Vamborg, F., Villaume, S. and Thépaut, J.N. (2020) The ERA5 global reanalysis. *Quarterly Journal of the Royal Meteorological Society*, 146(730), 1999–2049. <https://doi.org/10.1002/qj.3803>.
- Hong, C.-C. and Wu, Y.-K. (2018) Influence of climate regime shift on the abrupt change of tropical cyclone activity in various genesis regions. *Extreme Weather*. IntechOpen. 11–30. <https://doi.org/10.5772/intechopen.74947>.
- Hong, J.S., Yeh, S.W. and Seo, K.H. (2018) Diagnosing physical mechanisms leading to pure heat waves versus pure tropical nights over the Korean Peninsula. *Journal of Geophysical Research: Atmospheres*, 123(14), 7149–7160. <https://doi.org/10.1029/2018JD028360>.
- Horton, D.E., Johnson, N.C., Singh, D., Swain, D.L., Rajaratnam, B. and Diffenbaugh, N.S. (2015) Contribution of changes in atmospheric circulation patterns to extreme temperature trends. *Nature*, 522(7557), 465–469. <https://doi.org/10.1038/nature14550>.
- Hu, L. and Huang, G. (2020) The changes of high-temperature extremes and their links with atmospheric circulation over the Northern Hemisphere. *Theoretical and Applied Climatology*, 139(1–2), 261–274. <https://doi.org/10.1007/s00704-019-02970-1>.
- Hurrell, J.W., Holland, M.M., Gent, P.R., Ghan, S., Kay, J.E., Kushner, P.J., Lamarque, J.-F., Large, W.G., Lawrence, D., Lindsay, K., Lipscomb, W.H., Long, M.C., Mahowald, N., Marsh, D.R., Neale, R.B., Rasch, P., Vavrus, S., Vertenstein, M., Bader, D., Collins, W.D., Hack, J.J., Kiehl, J. and Marshall, S. (2013) The Community Earth System Model: a framework for collaborative research. *Bulletin of the American Meteorological Society*, 94(9), 1339–1360. <https://doi.org/10.1175/BAMS-D-12-00121.1>.
- Imada, Y., Watanabe, M., Kawase, H., Shiogama, H. and Arai, M. (2019) The July 2018 high temperature event in Japan could not have happened without human-induced global warming. *Scientific Online Letters on the Atmosphere*, 15, 8–12. <https://doi.org/10.2151/sola.15A-002>.
- Iturbide, M., Gutiérrez, J.M., Alves, L.M., Bedia, J., Cimadevilla, E., Cofiño, A., Cerezo-Mota, R., Di Luca, A., Faria, S.H., Gorodetskaya, I., Hauser, M., Herrera, S., Hewitt, H., Hennessy, K., Jones, R., Krakowska, S., Manzanas, R., Marínez-Castro, D., Narisma, G.T., Nurhati, I., Pinto, I., Seneviratne, S., van den Hurk, B. and Vera, C. (2020) An update of IPCC climate reference regions for subcontinental analysis of climate model data: definition and aggregated datasets. *Earth System Science Data Discussions*, 12(4), 2959–2970. <https://doi.org/10.5194/essd-12-2959-2020>.
- Kim, H.K., Moon, B.K., Kim, M.K., Park, J.Y. and Hyun, Y.K. (2021) Three distinct atmospheric circulation patterns associated with high temperature extremes in South Korea. *Scientific Reports*, 11(1), 1–14. <https://doi.org/10.1038/s41598-021-92368-9>.
- Kornhuber, K., Osprey, S., Coumou, D., Petri, S., Petoukhov, V., Rahmstorf, S. and Gray, L. (2019) Extreme weather events in early summer 2018 connected by a recurrent hemispheric wave-7 pattern. *Environmental Research Letters*, 14(5), 054002. <https://doi.org/10.1088/1748-9326/ab13bf>.
- Kysely, J. and Kim, J. (2009) Mortality during heat waves in South Korea, 1991 to 2005: How exceptional was the 1994 heat wave? *Climate Research*, 38(2), 105–116. <https://doi.org/10.3354/cr00775>.
- Lanzante, J.R. (1996) Resistant, robust and non-parametric techniques for the analysis of climate data: theory and examples, including applications to historical radiosonde station data. *International Journal of Climatology*, 16(11), 1197–1226. [https://doi.org/10.1002/\(SICI\)1097-0088\(199611\)16:11<1197::AID-JOC89>3.0.CO;2-L](https://doi.org/10.1002/(SICI)1097-0088(199611)16:11<1197::AID-JOC89>3.0.CO;2-L).
- Lawrence, D.M., Oleson, K.W., Flanner, M.G., Thornton, P.E., Swenson, S.C., Lawrence, P.J., Zeng, X., Yang, Z.-L., Levis, S., Sakaguchi, K., Bonan, G.B. and Slater, A.G. (2011) Parameterization improvements and functional and structural advances in version 4 of the Community Land Model. *Journal of Advances in Modeling Earth Systems*, 3(3), M03001. <https://doi.org/10.1029/2011MS000045>.
- Lee, H.J., Jeon, W., Lee, W.S. and Lee, H.W. (2021) Human-perceived temperature changes in South Korea and their association with atmospheric circulation patterns. *Journal of Climate*, 34(4), 1273–1290. <https://doi.org/10.1175/JCLI-D-20-0344.1>.
- Lee, W.S. and Lee, M.I. (2016) Interannual variability of heat waves in South Korea and their connection with large-scale atmospheric circulation patterns. *International Journal of Climatology*, 36(15), 4815–4830. <https://doi.org/10.1002/joc.4671>.
- Li, J., Zhu, Z. and Dong, W. (2017) Assessing the uncertainty of CESM-LE in simulating the trends of mean and extreme temperature and precipitation over China. *International Journal of Climatology*, 37(4), 2101–2110. <https://doi.org/10.1002/joc.4837>.

- Long, Y., Li, J., Zhu, Z. and Zhang, J. (2022) Predictability of the anomaly pattern of summer extreme high-temperature days over southern China. *Climate Dynamics*, 59(3–4), 1027–1041. <https://doi.org/10.1007/s00382-022-06170-y>.
- Luber, G. and McGeehin, M. (2008) Climate change and extreme heat events. *American Journal of Preventive Medicine*, 35(5), 429–435. <https://doi.org/10.1016/j.amepre.2008.08.021>.
- Luo, M. and Lau, N.C. (2019) Amplifying effect of ENSO on heat waves in China. *Climate Dynamics*, 52(5–6), 3277–3289. <https://doi.org/10.1007/s00382-018-4322-0>.
- Luo, M. and Lau, N.C. (2020) Summer heat extremes in northern continents linked to developing ENSO events. *Environmental Research Letters*, 15(7), 074042. <https://doi.org/10.1088/1748-9326/ab7d07>.
- Ma, S., Zhou, T., Stone, D.A., Angélil, O. and Shiogama, H. (2017) Attribution of the July–August 2013 heat event in central and eastern China to anthropogenic greenhouse gas emissions. *Environmental Research Letters*, 12(5), 054020. <https://doi.org/10.1088/1748-9326/aa69d2>.
- Meehl, G.A. and Tebaldi, C. (2004) More intense, more frequent, and longer lasting heat waves in the 21st century. *Science*, 305(5686), 994–997. <https://doi.org/10.1126/science.1098704>.
- Min, S.-K., Kim, Y.-H., Kim, M.-K. and Park, C. (2014) Assessing human contribution to the summer 2013 Korean heat wave. *Bulletin of the American Meteorological Society*, 95(9), S48–S51.
- Muller, R.A., Rohde, R., Jacobsen, R., Muller, E. and Wickham, C. (2013) A new estimate of the average earth surface land temperature spanning 1753 to 2011. *Geoinformatics & Geostatistics: An Overview*, 1(1), 1–7. <https://doi.org/10.4172/2327-4581.1000101>.
- Neale, R.B., Chen, C.-C., Gettelman, A., Lauritzen, P.H., Park, S., Williamson, D.L., Conley, A.J., Garcia, R., Kinnison, D., Lamarque, J.-F., Marsh, D., Mills, M., Smith, A.K., Tilmes, S., Vitt, F., Morrison, H., Cameron-Smith, P., Collins, W.D., Iacono, M.J., Easter, R.C., Liu, X., Ghan, S.J., Rasch, P.J. and Taylor, M.A. (2012) *Description of the NCAR Community Atmosphere Model (CAM 5.0)*. Boulder, CO: NCAR. Technical Note NCAR/TN-486+STR.
- Overland, J.E. and Wang, M. (2021) The 2020 Siberian heat wave. *International Journal of Climatology*, 41(S1), E2341–E2346. <https://doi.org/10.1002/joc.6850>.
- Park, J.-K., Jung, W.-S. and Kim, E.-B. (2008) A study on development of the extreme heat standard in Korea. *Journal of the Environmental Sciences*, 17, 657–669.
- Perkins, S.E. and Alexander, L.V. (2013) On the measurement of heat waves. *Journal of Climate*, 26(13), 4500–4517. <https://doi.org/10.1175/JCLI-D-12-00383.1>.
- Perkins, S.E., Alexander, L.V. and Nairn, J.R. (2012) Increasing frequency, intensity and duration of observed global heatwaves and warm spells. *Geophysical Research Letters*, 39(20), L20714. <https://doi.org/10.1029/2012GL053361>.
- Peterson, T.C., Zhang, X., Brunet-India, M. and Vázquez-Aguirre, J. L. (2008) Changes in North American extremes derived from daily weather data. *Journal of Geophysical Research: Atmospheres*, 113(7), D07113. <https://doi.org/10.1029/2007JD009453>.
- Rayner, N.A., Parker, D.E., Horton, E.B., Folland, C.K., Alexander, L.V., Rowell, D.P., Kent, E.C. and Kaplan, A. (2003) Global analyses of sea surface temperature, sea ice, and night marine air temperature since the late nineteenth century. *Journal of Geophysical Research: Atmospheres*, 108(14), 4407. <https://doi.org/10.1029/2002jd002670>.
- Ren, L., Ren, L., Zhou, T., Zhou, T., Zhou, T. and Zhang, W. (2020) Attribution of the record-breaking heat event over Northeast Asia in summer 2018: the role of circulation. *Environmental Research Letters*, 15(5), 054018. <https://doi.org/10.1088/1748-9326/ab8032>.
- Rodionov, S.N. (2004) A sequential algorithm for testing climate regime shifts. *Geophysical Research Letters*, 31(9), L09204. <https://doi.org/10.1029/2004GL019448>.
- Rodionov, S.N. (2006) Use of prewhitening in climate regime shift detection. *Geophysical Research Letters*, 33(12), L12707. <https://doi.org/10.1029/2006GL025904>.
- Smith, R., Jones, P., Briegleb, B., Bryan, F., Danabasoglu, G., Dennis, J., Dukowicz, J., Eden, C., Fox-Kemper, B. and Gent, P. (2010) *The parallel ocean program (POP) reference manual: ocean component of the community climate system model (CCSM) and community earth system model (CESM)*. Boulder, CO: NCAR/UCAR.
- Takaya, K. and Nakamura, H. (1997) A formulation of a wave-activity flux for stationary Rossby waves on a zonally varying basic flow. *Geophysical Research Letters*, 24(23), 2985–2988. <https://doi.org/10.1029/97GL03094>.
- Takaya, K. and Nakamura, H. (2001) A formulation of a phase-independent wave-activity flux for stationary and migratory quasigeostrophic eddies on a zonally varying basic flow. *Journal of the Atmospheric Sciences*, 58(6), 608–627. [https://doi.org/10.1175/1520-0469\(2001\)058<0608:AFOAPI>2.0.CO;2](https://doi.org/10.1175/1520-0469(2001)058<0608:AFOAPI>2.0.CO;2).
- Trenberth, K.E. and Fasullo, J.T. (2012) Climate extremes and climate change: the Russian heat wave and other climate extremes of 2010. *Journal of Geophysical Research: Atmospheres*, 117(17), D17103. <https://doi.org/10.1029/2012JD018020>.
- Vautard, R., Yiou, P., Otto, F., Stott, P., Christidis, N., Van Oldenborgh, G.J. and Schaller, N. (2016) Attribution of human-induced dynamical and thermodynamical contributions in extreme weather events. *Environmental Research Letters*, 11(11), 114009. <https://doi.org/10.1088/1748-9326/11/11/114009>.
- Vinnikov, K.Y., Robock, A., Stouffer, R.J., Walsh, J.E., Parkinson, C.L., Cavalieri, D.J., Mitchell, J.F.B., Garrett, D. and Zakharov, V.F. (1999) Global warming and Northern Hemisphere sea ice extent. *Science*, 286(5446), 1934–1937. <https://doi.org/10.1126/science.286.5446.1934>.
- von Storch, H. (1999) Misuses of statistical analysis in climate research. In: von Storch H and Navarra A (eds), *Analysis of Climate Variability*. Berlin-Heidelberg: Berlin, Heidelberg, 11–26. <https://doi.org/10.1007/978-3-662-03744-7>.
- Wang, J., Chen, Y., Tett, S.F.B., Yan, Z., Zhai, P., Feng, J. and Xia, J. (2020) Anthropogenically-driven increases in the risks of summertime compound hot extremes. *Nature Communications*, 11(1), 528. <https://doi.org/10.1038/s41467-019-14233-8>.
- Xia, J., Tu, K., Yan, Z. and Qi, Y. (2016) The super-heat wave in eastern China during July–August 2013: a perspective of climate change. *International Journal of Climatology*, 36(3), 1291–1298. <https://doi.org/10.1002/joc.4424>.
- Xu, P., Wang, L., Liu, Y., Chen, W. and Huang, P. (2020) The record-breaking heat wave of June 2019 in Central Europe. *Atmospheric Science Letters*, 21(4), e964. <https://doi.org/10.1002/asl.964>.

- Yeh, S.W., Lee, E.H., Min, S.K., Lee, Y.H., Park, I.H. and Hong, J.S. (2021) Contrasting factors on the trends in hot days and warm nights over Northern Hemisphere land during summer. *Weather and Climate Extremes*, 34, 100389. <https://doi.org/10.1016/j.wace.2021.100389>.
- Yeh, S.W., Won, Y.J., Hong, J.S., Lee, K.J., Kwon, M., Seo, K.H. and Ham, Y.G. (2018) The record-breaking heat wave in 2016 over South Korea and its physical mechanism. *Monthly Weather Review*, 146(5), 1463–1474. <https://doi.org/10.1175/MWR-D-17-0205.1>.
- Yeo, S.R., Yeh, S.W. and Lee, W.S. (2019) Two types of heat wave in Korea associated with atmospheric circulation pattern. *Journal of Geophysical Research: Atmospheres*, 124(14), 7498–7511. <https://doi.org/10.1029/2018JD030170>.
- Zhang, G., Zeng, G., Li, C. and Yang, X. (2020) Impact of PDO and AMO on interdecadal variability in extreme high temperatures in north China over the most recent 40-year period. *Climate Dynamics*, 54(5–6), 3003–3020. <https://doi.org/10.1007/s00382-020-05155-z>.
- Zhou, T., Shuangmei, M. and LiWei, Z. (2014) Understanding a hot summer in central eastern China: summer 2013 in context of multimodel trend analysis. *Bulletin of the American Meteorological Society*, 95(9), S54–S57.
- Zhu, Z. and Li, T. (2017) The record-breaking hot summer in 2015 over Hawaii and its physical causes. *Journal of Climate*, 30(11), 4253–4266. <https://doi.org/10.1175/JCLI-D-16-0438.1>.
- Zhu, Z. and Li, T. (2018) Extended-range forecasting of Chinese summer surface air temperature and heat waves. *Climate Dynamics*, 50(5–6), 2007–2021. <https://doi.org/10.1007/s00382-017-3733-7>.

How to cite this article: Lee, Y.-H., Yeh, S.-W., Hong, J.-S., Shin, J., & An, S.-I. (2023). Regime shift increase in East Asia's summer extreme hot day frequency across the late 1990s. *International Journal of Climatology*, 43(5), 2305–2317. <https://doi.org/10.1002/joc.7976>